Light Metals 2014
Edited by: John Grandfield
TMS (The Minerals, Metals & Materials Society), 2014

RODDING IN HALL-HÉROULT CELLS: AN FEA MODEL THAT PREDICTS ROOM TEMPERATURE MECHANICAL PROPERTIES AND CRACKING TENDENCY OF THIMBLES

D.R. Gunasegaram, D. Molenaar
Commonwealth Scientific and Industrial Research Organisation (CSIRO)
Private Bag 33, Clayton (Melbourne), Victoria, Australia, 3169

Keywords: Finite Element Analysis, Hall-Héroult Cell, Stub to Carbon Voltage Drop, Hypereutectic Gray Cast Iron, Solidification, Fracture.

Abstract

The quality and extent of the contact between the thimble and the anode comprising the anode assembly of a Hall-Héroult cell are influenced by the mechanical properties of the thimble. The contact is established when the thimble differentially expands with increasing temperature during the cell start-up phase and touches the anode surface. The size and shape of the contact area and the magnitude of the interfacial pressure are subsequently modified as the thimble deforms with further increases in temperature. Crucially, this deformation mechanism is complicated by the fact that the thimble properties vary from location to location based on processing history unique to each location. It is therefore necessary to account for such variations if realistic predictions are to be made for electrical and thermal flux profiles across the critical thimble-anode interface. In the present work, a fully coupled transient thermal-mechanical model is developed for thimble solidification using the finite element code Abaqus. This continuum scale model predicts the local mechanical properties of the slightly hypereutectic gray iron casting at room temperature by recreating the phase fractions based on local non-equilibrium cooling rates. These properties may be modified for elevated temperatures using experimentally obtained relationships available in the literature. The model also predicts the cracking tendency of the solidifying thimble based on calculated equivalent plastic strain profiles. The computation time for this model is relatively short.

Introduction

About one third [1] of the voltage drop experienced across the entire anode assembly of a Hall-Héroult aluminum reduction cell is accounted for by the stub-to-carbon (STC) voltage drop that extends across the stub-thimble and thimble-carbon (anode) interfaces (Fig. 1). The slightly hypereutectic gray cast iron thimble shrinks onto the steel stub during solidification in the rodding stage and ensures intimate contact between the two components. However, during thermal contraction, an air gap forms between the thimble and the carbon anode (Fig. 1). It only partially closes during the subsequent differential expansion caused by the rising temperature of the anode assembly following setting into the hot reduction cell. Thus, the rate-controlling influence of the thimble-anode interface dominates the STC voltage drop. It follows that any improvements made in modeling this interface would have a significant impact on the accuracy of the overall model.

The spread of the electrical and thermal fluxes across the thimble-anode interface and their magnitudes are determined by the coverage and degree of contact at any given time. These contact conditions are dependent in part on the deformation behavior of the thimble. Consequently, by accounting for the spatial dependence of the mechanical properties of the thimble in the model, the representation of the thimble-anode interface may be improved.

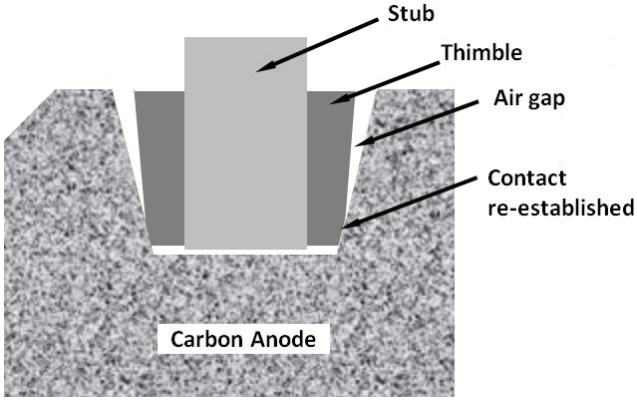

Figure 1. Cross sectional view of the thimble-anode interface during the cell operation phase where there is partial contact between the two components.

The mechanical properties of a casting for a given composition are derived from the local microstructures that evolve as a response to the cooling history associated with the location. The local cooling rate in a solidifying casting is determined by various parameters including the surrounding section thickness and the heat transfer efficiency in the vicinity. A simulation of the casting process can account for the influence of such factors in calculating the local cooling rates. Microstructures may accordingly be assigned to the various locales based on experimentally obtained cooling rate vs. microstructure relationships for the alloy composition. It is then possible to estimate the mechanical properties at various locations in accordance with the prescribed microstructures.

It is also beneficial for the model to predict the cracking tendency of thimbles during the rodding stage. These cracks are presumably the result of a stress-relieving mechanism that initiates as hot tears in the advanced stage of solidification when access to feed metal has ceased. Hot tears develop as a result of (i) thermal strains resulting from the differential contraction of adjacent sections of the casting, and (ii) mechanical strains attributable to geometric constraints presented by the mold. Cracks in the solidified casting do not necessarily make it unfit for use; in fact within the industry it is considered suitable to have one, two or even three observable cracks in the thimble at the completion of the rodding stage. However, knowing if and where cracks would form will provide a

distinctive advantage to the smelter engineers as the presence of cracks may alter the contact characteristics between components that form the STC connection.

In the present work, a fully coupled transient thermal-mechanical finite element model was developed in the continuum scale for the solidification process. The model is capable of predicting room temperature mechanical properties based on a simulated distribution of phase fractions. It also predicts the likely locations where cracks may initiate within the thimbles based on calculated equivalent plastic strain profiles. Important features of this model include the following: (a) its predictions are relevant to non-equilibrium solidification rates and the finer microstructures common to real world situations, and (b) its relative short computation times make it attractive for use in applications related to commercial operations.

Literature Review

The conclusions from the literature review are presented under separate headings below.

Continuum models for microstructure prediction

The review highlighted a scarcity of continuum scale solidification models capable of predicting mechanical properties for the specialized case of hypereutectic gray cast iron solidifying under non-equilibrium cooling conditions. However, multiscale microstructural models for nodular cast iron (e.g. [2-3]) and gray cast iron hypoeutectic compositions [4-6] are available and similar models for hypereutectic compositions are being developed by CSIRO and partners [7]. Nonetheless, all of these were developed for equilibrium or near-equilibrium cooling conditions based on equilibrium phase diagrams and in some cases had limited validation carried out. These solidification conditions were far removed from those experienced in real world industrial processes. In addition, their computational load was relatively high due to the large amount of detail incorporated in the microscopic scale. Thus, a computationally light single-scale continuum model for the prediction of microstructure, mechanical properties and cracking tendency in hypereutectic gray cast irons solidifying at industrially relevant cooling rates appears not to exist.

Models incorporating spatially varying mechanical properties

No existing model simulating cell operation incorporated spatially varying mechanical properties for the thimble material. In addition, the only model comprising the anode assembly that simulated the cell start-up and operation phases realistically as transient processes was by the current authors [1].

Cooling rate vs. microstructure relationship

Multiscale microstructural models employ various schemes for the nucleation and growth of phases during the solidification of cast irons. However, it was difficult to find data on how the phase fractions changed with high cooling rates, as most of the models were developed for slow cooling conditions. This was especially true for the hypereutectic compositions, which were hardly investigated. The finding is perhaps unsurprising when considering the fact that the results would change with each small variation in composition, meaning that a myriad of experiments will need to be carried out to generate the required data. Furthermore, there were no Time-Temperature-Transformation (TTT) diagrams available for hypereutectic compositions. Thus, there is a need to generate experimental data for those compositions at non-equilibrium cooling rates.

Prediction of locations vulnerable to cracking tendency

Any major attempt at simulating the cracking behavior of thimbles should incorporate a phenomenological elastic-viscoplastic model for cast iron behavior. This is because conventional models such as the von Mises plasticity model do not account for plastic volume change, and thus do not allow damage to be predicted [8]. However, (a) such a model does not exist in the open domain for hypereutectic compositions and (b) its use in simulations will significantly add to the computational load of the model. Therefore, it is prudent in the present work to obtain the cracking tendency of the material using the equivalent plastic strains predicted using elastic-plastic material properties.

Aim and Modeling Strategy

The aim of the work was to develop a three-dimensional fully coupled thermal-mechanical transient model in the continuum scale for the rodding process that would predict: (i) the room temperature phase fractions and mechanical properties of the hypereutectic gray cast iron thimble casting based on processing history, and (ii) the locations on thimbles most susceptible to the initiation of cracks based on calculated equivalent plastic strain. In this paper, the emphasis is placed on discussing the capabilities of the model rather than on the validation of its predictions.

The rodding process involves two-way couplings between the thermal and mechanical physics, and so must be modeled as such for realistic predictions of the air gap (see discussion in [1]). This coupling was achieved in the present simulations through the use of fully coupled thermal-mechanical hexahedral elements C3D8T in Abaqus v6.13.

The calculations of the phase fractions and mechanical properties were carried out during the analysis using user-subroutine USDFLD. These values related to the final state of the casting at room temperature rather than to any stage during solidification, and thus were not used as real-time inputs to the rodding simulation. The calculation of strains relating to the cracking tendency was independently carried out within Abaqus.

Before the analysis, the entire geometry was solid modeled as an assembly of parts - without any gaps between the thimbles and the anode. Half symmetry was utilized to employ a larger number of (smaller) elements. This is a course of action that generally improves accuracy of predictions. The solution scheme that was used is illustrated in Fig. 2.

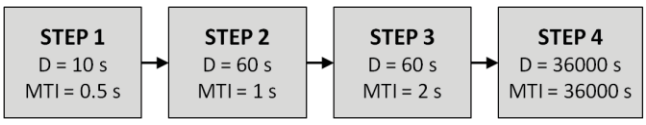

Figure 2. Modeling strategy used.
D = Duration (of step) and MTI = Maximum Time Increment.

The rodding stage, spanning just over 10 h (to cool to room temperature of 300 K), was divided into four different steps so that time increments could be progressively increased. Although highly conservative, such control of time increments at early stages of solidification is desirable for capturing the cooling

histories of nodes accurately – since temperatures reduce rapidly at the start of solidification. Accurate cooling histories were required to obtain realistic estimates of cooling rates, which were pivotal to phase fraction calculations.

Description of the Model

Software and Hardware

Abaqus/Standard v6.13 was run on a single compute node with 12 processors in a shared memory environment at the CSIRO High Performance Computing Centre. The direct solver was used with 12 domains with full integration for the Newton-Raphson solution scheme.

Geometry

The geometry (Fig. 3) comprised an assembly that included a stub, a thimble and the anode, with no cast iron volume beneath the stub. While the parts resembled those used in some commercial pre-baked anode technologies, the thimble geometry was deliberately created to represent a generic design with comparable section volumes and thicknesses.

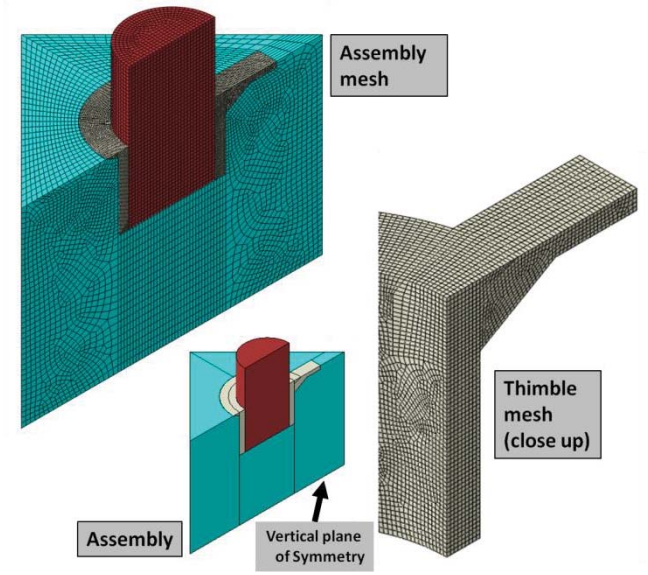

Figure 3. Geometry and mesh used for simulations. Colors depict various materials.

Mesh statistics

Details of the fully hexahedral mesh used are presented in Table I and shown in Fig. 3. All elements were 8-noded, each with 8 integration points where quantities are calculated. As shown in the close up view of the thimble mesh, there were 9 elements across the 18 mm thickness of the annular wall of the thimble. This was considered sufficient to capture the relatively large temperature gradients across this wall.

Material Properties

Materials designated for the parts are listed in Table II. Temperature-dependent material properties obtained from the public domain were used for most materials. For the thimble material, custom data on thermal expansion coefficient was generated at CSIRO. Whilst the thimble and stub materials were assumed to display elastic-plastic behavior, the anode material was modeled as a purely linear elastic entity.

Table I. Mesh statistics

Part	Number of Nodes	Element Type	Number of Elements	Typical Edge Length of Element (m) Fine/Coarse
Anode	78918	C3D8T	73646	0.004/0.017
Thimble	91666	C3D8T	17940	0.002/0.002
Stub	20069	C3D8T	79855	0.005/0.005
TOTAL	190653		171441	

Table II. Material designations for parts

Part	Material
Anode	Baked anode carbon
Thimble	Gray cast iron
Stub	SAE1020

Thermal boundary conditions and initial conditions

Typical heat transfer coefficients were defined for calculating heat exchange between the solid bodies and their local ambient (see Table III). Radiation from the hot gray cast iron melt was also modeled.

Table III. Heat transfer parameters and initial conditions.

Interface	Heat Transfer Coefficient ($Wm^{-2}K^{-1}$) at [gap] (m)
CONDUCTIVE	
Thimble-anode	500 [0.0] 500 [0.0005] 0 [0.001]
Thimble-stub	2500 [0.0] 1500 [0.0005] 0 [0.005]
Stub-anode	Same as thimble-anode above
CONVECTIVE All surfaces exposed to the ambient (300 K or 27 ºC) were assumed to lose heat by convection	50
RADIATIVE The top surface of the cast iron was assumed to radiate to the ambient at 300 K (27 ºC)	Emissivity 0.9
INITIAL CONDITIONS Thimble initial temperature Anode and stub initial temperature	 1673 K (1400 ºC) 300 K (27 ºC)

Mechanical boundary conditions

The floor on which the anode rested was defined by restricting the vertical (y-direction) movements of nodes at the bottom surface of the anode. The vertical plane of symmetry (Fig. 3) was restricted in displacements in the x-direction normal to the plane, as well as in rotations about y- and z- axes.

For contact, a penalty frictional formulation was used. The coefficient of friction was assumed to be 0.2 at the stub-anode and thimble-anode interfaces, and 0.5 at the thimble-stub interface. Finite sliding in the tangential direction and hard pressure overclosure in the normal direction was assumed.

Loads

To keep the stub in contact with the anode, a small pressure load (1 MPa) was applied on the top surface of the stub. This was expected to not have any influence on results.

Calculation of local phase fractions

The assignment of phase fractions at an integration point on a cast iron element is a necessary precondition for determining the mechanical properties at that point. In turn, the mix of phases expected at an integration point are determined by the cooling rate at that point for a given alloy composition. Thus, the first calculation finds the cooling rate (ºC/s), which is calculated as:

$$CR = (T_l - T_s)/ (t_l - t_s) \quad (1)$$

where T_l (=1563 K) and T_s (=1448 K) are liquidus and solidus temperatures respectively, and t_l and t_s are the time points at which cast iron at an integration point passes through T_l and T_s, respectively. The next step is to assign the phase fractions. For this one needs to consider that room temperature microstructures for slightly hypereutectic compositions contain graphite (as flakes), ferrite, pearlite (which comprises 12 % cementite and 88 % ferrite according to the lever rule) and cementite. These fractions may be ascertained from metallography. In addition, these phases must be correlated with the cooling rates responsible for their formation. It was possible in our case to establish the cooling rate at which the phase fraction would be 100 % cementite (manifesting as a thick white layer on a fracture surface) without metallography. For this, a chill wedge fracture surface obtained in the CSIRO foundry was compared against a simulation of its cooling rate (Fig. 4). The cooling rate above which the entire material transformed into cementite was thus estimated as CR > 45 ºC/s.

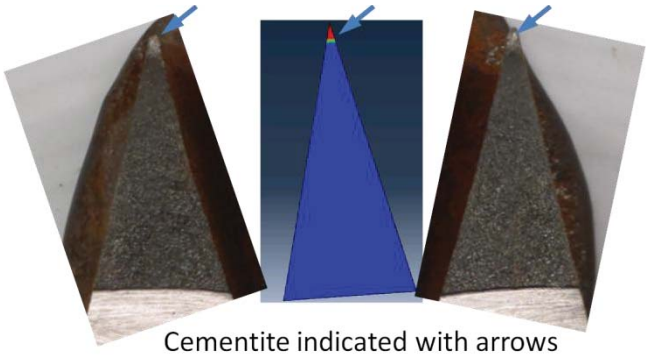

Figure 4. The white color on the narrow tip of the fracture surfaces of chill castings (either side) is compared against calculated cooling rates (depicted using color, center).

For the remaining phases, metallographic characterization data has to be generated for the various locations in the casting following physical casting trials involving the non-equilibrium cooling of thimbles. Cooling rates may then be associated with phase fraction data for each of the locations using values calculated from simulations as before and/or using thermocouple data logged during experimentation. Until such custom data is generated, an assumed rule (Table IV) based on expected trends may be used. As the emphasis on the present work was on highlighting the capabilities of the model rather than on providing validated results, this approach was justified.

Calculation of local mechanical properties

Room temperature mechanical properties were assumed to be directly related to room temperature phase fractions. Using mechanical properties for the individual phases obtained from the public domain (Table V), the properties at the integration points were calculated as weighted fractions of the phases.

Table IV. The relationship between phases and cooling rates used in the model for a slightly hypereutectic gray cast iron composition.

Cooling rate (ºC/s)	Cementite	Ferrite	Graphite	Total
0	9.6	70.4	20.0	100
5	24.0	66.0	10.0	100
40	64.2	30.8	5.0	100
45	100.0	0.0	0.0	100

Table V. Mechanical properties of phases

Phase	Ultimate tensile strength (UTS) (Pa)	Elongation (%)	Brinell Hardness
Cementite	450×10^6	0.05%	410.0
Ferrite	291×10^6	0.60%	125.0
Graphite	28×10^6	0.00%	2.5

Results and Discussion

Run times

The entire simulation comprising the rigorous four step scheme (Fig. 2) was completed in 49 h 40 m (but took only 19 h 40 m when the casting process was simulated as a single step without restrictions on the time step size). The virtual memory usage was 36.1 GB. If lower computation times are required, the highly conservative 4-step scheme may be relaxed and/or the number of elements in the model reduced. If that were the case, any potential implications for the accuracy of predictions need to be determined using sensitivity studies.

Cooling rate predictions

Cooling rates predicted by the model are shown in Fig. 5. As expected, the parts of the casting which are in intimate contact with the stub and the tip region of the collar section solidified most rapidly. The cooling rates near the thimble-anode interface are lower, partly due to the insulating air gap and partly due to the lower thermal conductivity of carbon when compared with steel. Clearly the slowest cooling rate is within the thickest section of the thimble at the junction of the pouring sprue.

Phase fraction predictions

Phase fractions predicted by the model based on the relationship to cooling rates (Table IV and Fig. 5) are presented in Figs. 6-8. It was possible to validate the predictions relating to cementite (Fig. 6) using a fractured surface of an industrial thimble (Fig. 9) of a similar size and composition. It can be seen that the cementite manifesting as a white layer on that surface on its concave side is approximately the same size as the red color shading on the corresponding area (see inset of Fig. 6), which indicates a cementite fraction of close to 100 % in the predictions. Thus the predictions are in agreement with reality. A large amount of cementite was also predicted at the tip of the collar, again as expected. Due to the lower cooling rates at the thimble-anode interface regions, lower amounts of cementite were predicted there. This was confirmed to be the case in reality by the absence of a white layer on the fracture surface on its convex side (Fig. 9).

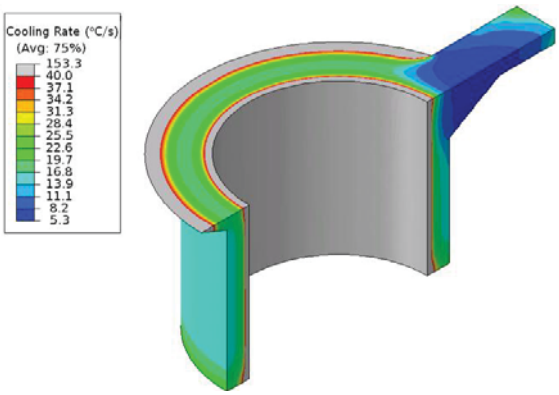

Figure 5. Predicted cooling rates (ºC/s).

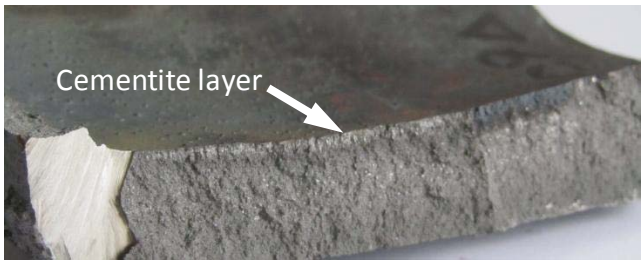

Figure 9. Fracture surface of an industrial thimble where a layer of white is seen in areas adjoining the thimble-stub interface.

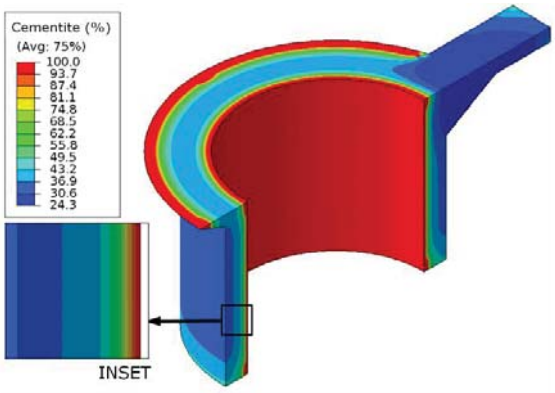

Figure 6. Predicted cementite phase fraction (%).

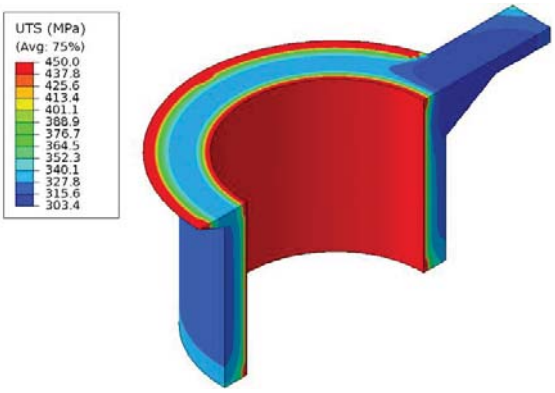

Figure 10. Predicted ultimate tensile strength (MPa).

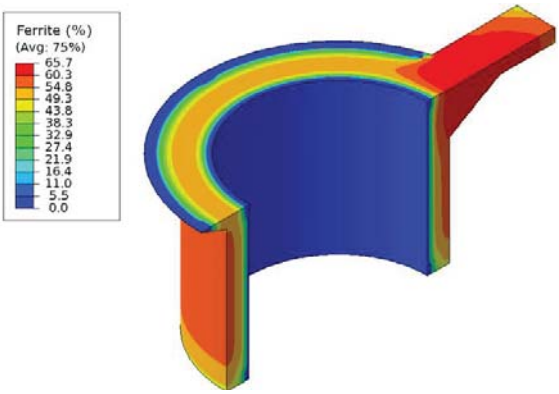

Figure 7. Predicted ferrite phase fraction (%).

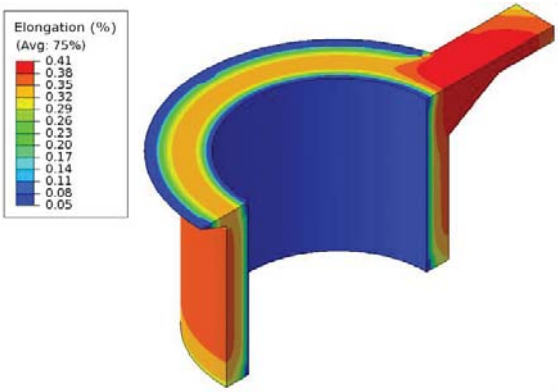

Figure 11. Predicted elongation (%).

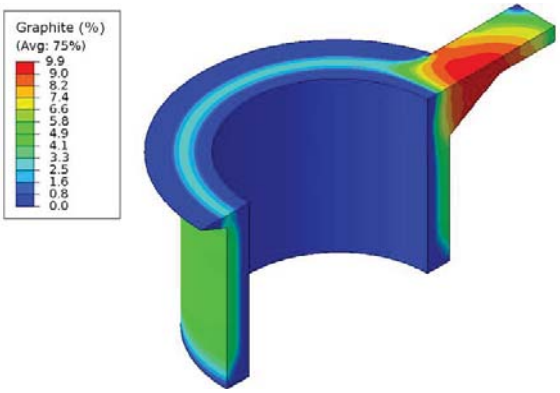

Figure 8. Predicted graphite phase fraction (%).

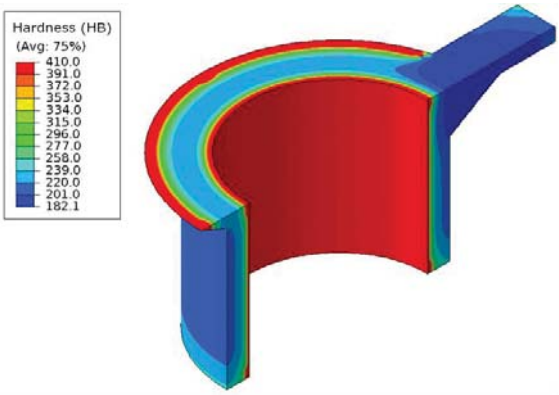

Figure 12. Predicted hardness (HB).

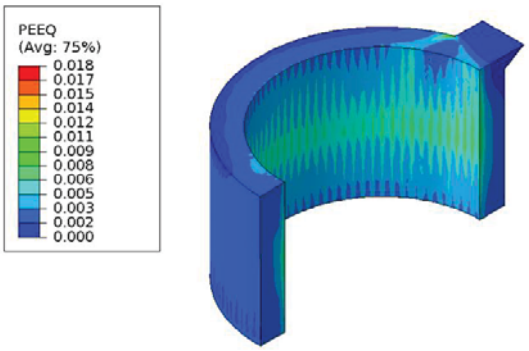

Figure 13. Predicted equivalent plastic strain (-).

Figure 14. Validation of the predicted equivalent plastic strain based on a crack observed in an industrial thimble.

Mechanical property predictions

Mechanical properties predicted by the model are shown in Figs. 10-12. The properties vary as expected, e.g. high cementite regions were estimated to have higher ultimate tensile strength (UTS) and hardness but lower elongation. Similarly, high graphite regions are predicted to have lower mechanical properties.

It is appropriate to point out here that, although room temperature mechanical properties were predicted by the present model, these may be adjusted for elevated temperatures based on published data. For instance, it is known that the UTS of gray cast iron (assumed as a homogeneous whole, without distinguishing between phases) remains largely unchanged at about 325 MPa from room temperature to about 400 ºC, above which it decreases linearly to reach about 100 MPa at 650 ºC [9]. Using the same ratio (=100/325 =0.31), regions with a predicted UTS of, say, 440 MPa at room temperature may be expected to have a value of 135 MPa at 650 ºC. Whilst clearly this is an approximation, the strategy may be used until accurate elevated temperature data becomes available.

Prediction of location(s) for potential crack formation

The equivalent plastic strain predictions, responsible for hot tears leading to cracking, are shown in Fig. 13. A slice on a horizontal plane where the maximum value of strain was predicted (inside the body of the casting) was selected for the figure. It can be seen that the region with the elevated strain levels extends across the thickness of the thimble. These strains are partly due to the constraint provided by the stub onto which the casting shrinks. The balance of the contributions are from thermal strains introduced by the large mismatch in thermal contractions experienced by the casting in the vicinity of the large thermal mass in the form of the pouring sprue. The prediction of the location is validated by comparing it to an actual crack on an industrial thimble (Fig. 14). It is observed that the predicted and actual locations match well, providing further confidence in the model.

Concluding Remarks

A fully coupled three-dimensional transient thermal-mechanical finite element model that simulates the rodding of the anode assembly in Hall–Héroult cells was developed. The computationally efficient model calculated the cooling rates and the resulting phase fraction distribution in the thimble casting for a slightly hypereutectic alloy. The phase fraction data was used by the model to predict room temperature mechanical properties at various locations in the casting. It was also capable of predicting the location on thimbles that was most vulnerable to cracking during the rodding process. Its predictions of cementite formation and cracking tendency were satisfactorily validated. It is intended that this model would be progressively refined with the use of more realistic inputs, especially for the relationship between cooling rate and phase fractions.

Acknowledgements

N. Alam of CSIRO provided helpful suggestions on the estimated phase fraction data (Table IV). Pacific Aluminium is thanked for permitting the use of images reproduced as Figs. 9 and 14. This project was sponsored by the CSIRO Minerals Down Under Flagship.

References

1. D.R Gunasegaram and D. Molenaar, "A fully coupled thermal-electrical-mechanical transient FEA model for a 3D anode assembly", *Light Metals 2013*, 1341-1346.
2. P.M. Dardati, D.J. Celentano, L.A. Godoy, A.A. Chiarella and B.J. Schulz, "Analysis of ductile iron solidification: numerical simulation and experimental validation", *International Journal of Cast Metals Research*, 22 (2009), 390-400.
3. D.J. Celentano, P.M. Dardati, F.D. Carzaro and L.A. Godoy, Thermomechanical-microstructural modeling of nodular cast iron solidification", *Materials Science & Technology*, 29 (2013), 156-164.
4. D.J. Celentano, M.A. Cruchaga and B.J. Schulz, "On the effect of natural convection on the thermal-microstructural evolution in gray cast iron solidification", *Metallurgical and Materials Transactions B*, 37B (2006), 253-264.
5. D. Maijer, S.L. Cockcroft and W. Patt, "Mathematical modeling of microstructural development in hypoeutectic cast iron", *Metallurgical and Materials Transactions A*, 30A (1999), 2147-2158.
6. A. Jacot, D. Maijer and S. Cockcroft, "Modeling of microstructure and residual stress in cast iron calendar rolls", *Metallurgical and Materials Transactions A*, 31A (2000), 1201-1211.
7. A. Urrutia, D.J. Celentano, D.R. Gunasegaram and N. Deeva, "Thermal microstructural simulation of solidification and eutectoid transformation of hypereutectic gray cast iron", unpublished research.
8. M.G. Pokorny, C.A. Monroe and C. Beckermann, "Prediction of deformation and hot tear formation using a viscoplastic model with damage", *Shape Casting: The 3rd International Symposium*, 2009, 265-272.
9. J.R. Davis et. al. (Eds.), ASM Metals Handbook, Vol. 1, Properties and Selection: Irons, Steels and High Performance Alloys, 1990.